



HAL
open science

Vibroacoustic response of panels under diffuse acoustic field excitation from sensitivity functions and reciprocity principles

Christophe Marchetto, Laurent Maxit, Olivier Robin, Alain Berry

► **To cite this version:**

Christophe Marchetto, Laurent Maxit, Olivier Robin, Alain Berry. Vibroacoustic response of panels under diffuse acoustic field excitation from sensitivity functions and reciprocity principles. *Journal of the Acoustical Society of America*, 2017, 141 (6), pp.4508 - 4521. 10.1121/1.4985126 . hal-01710837

HAL Id: hal-01710837

<https://hal.science/hal-01710837>

Submitted on 16 Feb 2018

HAL is a multi-disciplinary open access archive for the deposit and dissemination of scientific research documents, whether they are published or not. The documents may come from teaching and research institutions in France or abroad, or from public or private research centers.

L'archive ouverte pluridisciplinaire **HAL**, est destinée au dépôt et à la diffusion de documents scientifiques de niveau recherche, publiés ou non, émanant des établissements d'enseignement et de recherche français ou étrangers, des laboratoires publics ou privés.

Vibroacoustic response of panels under diffuse acoustic field excitation from sensitivity functions and reciprocity principles

Christophe Marchetto* and Laurent Maxit

Univ Lyon, INSA-Lyon, Laboratoire Vibrations Acoustique, F-69621 Villeurbanne, France

Olivier Robin and Alain Berry

*Groupe d'Acoustique de l'Université de Sherbrooke,
Université de Sherbrooke, Sherbrooke, J1K 2R1, Canada*

(Dated: May 11, 2017)

Abstract

This paper aims at developing an experimental method to characterize the vibroacoustic response of a panel to a diffuse acoustic field excitation with a different laboratory setup than those used in standards (*i.e.*, coupled rooms). The proposed methodology is based on a theoretical model of the diffuse acoustic field and on the measurement of the panel's sensitivity functions which characterize its vibroacoustic response to wall plane waves. These functions can be estimated experimentally using variations of the reciprocity principle which are described in the present paper. These principles can either be applied for characterizing the structural response by exciting the panel with a normal force at the point of interest or for characterizing the acoustic response (radiated pressure, acoustic intensity) by exciting the panel with a monopole and a dipole source. For both applications, the validity of the proposed approach is numerically and experimentally verified on a test case composed of a baffled simply supported plate. An implementation for estimating the sound transmission loss of the plate is finally proposed. The results are discussed and compared with measurements performed in a coupled anechoic-reverberant room facility following standards.

PACS numbers: PACS: 43.40.At, 43.40.Dx

* christophe.marchetto@usherbrooke.ca

1 I. INTRODUCTION

2 The experimental vibroacoustic characterization of panels under a diffuse acoustic field
3 (DAF) excitation is of great interest for the industry. This excitation is commonly used
4 to determine the sound reduction index of panels as described in several standards using
5 coupled reverberant-reverberant room [1] [2] or reverberant-anechoic room [3] [4] laboratory
6 facilities. Theoretically, a DAF is defined as an infinite set of uncorrelated plane waves with
7 uniformly distributed incidence angles. In standard laboratory measurements, this excita-
8 tion is reproduced using a reverberant room and only partially corresponds to its theoretical
9 definition, especially below the Schroeder frequency of the room where the sound field is
10 dominated by well-defined acoustic cavity modes. Even above the Schroeder frequency, the
11 pressure field is not perfectly homogeneous and the lack of grazing incidence plane waves
12 has been pointed out in the literature. Inter-laboratory variations of vibroacoustic measure-
13 ments in reverberant rooms can be attributed to these phenomena, but other parameters
14 are involved such as room dimensions, niche effects, panel mounting conditions, aperture
15 size and measuring protocols [5] [6] [7].

16 In this context, the aim of this study is to investigate an alternative and robust approach
17 to experimentally characterize a panel's response to a DAF excitation by using only the
18 theoretical model of this excitation to overcome the limitations of a reverberant room mea-
19 surement discussed above. Indeed, the mathematical formulation of a panel's vibro-acoustic
20 response when submitted to random excitations in the wavenumber domain allows estimat-
21 ing the system's response, at any point on the structure or in the acoustic medium, from
22 wall-pressure cross spectral density (CSD) functions (characterizing the excitation) and from
23 so-called 'sensitivity functions', which were introduced in [8] [9] for the analogous problem
24 of panels excited by a turbulent flow. The latter are defined as the panel's response to wall-
25 pressure plane waves and characterize the panel's vibroacoustic behavior. The estimation of
26 the panel's response submitted to a DAF excitation therefore only requires the experimental
27 measurement of sensitivity functions in the acoustic wavenumber domain.

28 A method is proposed for estimating the sensitivity functions experimentally. Whereas
29 the direct interpretation of the sensitivity functions would require exciting the panel by sets
30 of wall plane waves, which is not easy from an experimental point of view, an alternative
31 method based on a reciprocity principle is proposed. The reciprocity principle states that the

32 sensitivity functions at any point on the structure or in the acoustic medium are equivalent
 33 to the panel's velocity response expressed in the wavenumber domain when the system is
 34 excited by a vibration or acoustic source at the same point. From an experimental point
 35 of view, it is then only necessary to excite the system with a vibration or acoustic source
 36 and to apply a wavenumber transform to the measured transfer function between the panel
 37 velocity and the source magnitude to obtain the sensitivity functions for a wide range of
 38 wavenumbers. Globally, the proposed experimental process consists in exciting the panel
 39 with the source of given magnitude at the point of interest. The spatial vibratory response of
 40 the panel is then measured with a scanning laser vibrometer. In a subsequent post-processing
 41 phase, a discrete 2-D wavenumber transform of the measured vibratory field is performed to
 42 deduce the sensitivity functions. Finally, using the wall-pressure model of a DAF and the
 43 previously estimated sensitivity functions, the response when the panel is excited by a DAF
 44 can be deduced at any point on the structure or in the acoustic medium. To evaluate the
 45 sound transmission loss, this process is repeated for a series of points belonging to a surface
 46 surrounding the panel to estimate the acoustic intensity at these points when the panel is
 47 excited by a DAF.

48 The remainder of the paper is organized as follows: the considered vibro-acoustic problem
 49 and the quantities characterizing a panel under a DAF are described in Sec. II. Then, the
 50 mathematical formulation of the vibro-acoustic problem is presented in Sec. III where the
 51 sensitivity functions appearing in the formulation are defined. An alternative interpretation
 52 of these functions based on the reciprocity principle is proposed in Sec. IV. This inter-
 53 pretation suggests a simple implementation for measuring the sensitivity functions. The
 54 proposed methodology for characterizing the panel response under a diffuse acoustic field
 55 is summarized in Sec. V. Numerical and experimental validations are provided in Sec. VI.
 56 Finally, a comparison with measurements performed following standards [4] is proposed in
 57 Sec. VII.

58 **II. VIBROACOUSTIC CHARACTERIZATION OF PANELS UNDER DIFFUSE** 59 **ACOUSTIC FIELD**

60 Let us consider a baffled panel of surface Σ_p with arbitrary boundary conditions separating
 61 two semi-infinite acoustic domains. Each of these acoustic domains is characterized by a

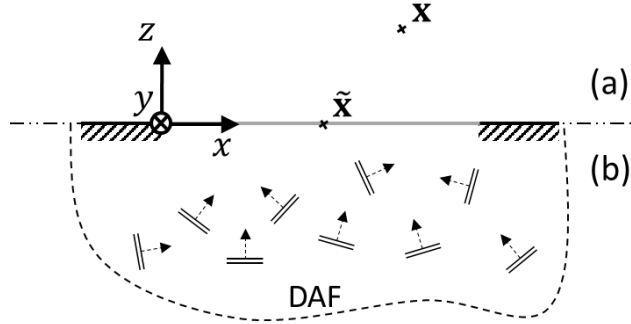


FIG. 1. Panel (gray line) and coordinate system. (a) receiving side: semi-infinite domain. (b) source side: theoretical DAF.

62 mass density ρ_0 and a sound velocity c_0 . As shown in Fig. 1, one supposes that a DAF is
 63 generated on one side of the panel. We define $\mathbf{x} = (x, y, z)$ the observation point in the
 64 receiving half space $z > 0$ or on the panel $z = 0$ and $\tilde{\mathbf{x}} = (\tilde{x}, \tilde{y})$ the excitation point on the
 65 panel surface. Both points are defined in the Cartesian coordinate system (x, y, z) shown in
 66 Fig. 1.

67 To experimentally characterize the vibroacoustic behavior of this panel, two quantities
 68 are considered:

- 69 - the one-sided normal velocity frequency response v at a given point on the panel,
 70 which for random excitations is given by the auto spectral density (ASD) function of
 71 the normal velocity $G_{vv}(\mathbf{x}, f)$,
- 72 - the transmission loss (TL) defined by

$$TL(f) = 10 \log_{10} \left(\frac{\Pi_{inc}(f)}{\Pi_{rad}(f)} \right), \quad (1)$$

73 where f is the frequency and is considered positive.

74 The incident acoustic power and the radiated acoustic power are denoted Π_{inc} and Π_{rad} , re-
 75 spectively. For a DAF exciting a panel of area Σ_p , the incident acoustic power is theoretically
 76 given by [10]

$$\Pi_{inc}(f) = \frac{G_{p_b p_b}(f) \Sigma_p}{8 \rho_0 c_0}, \quad (2)$$

77 where $G_{p_b p_b}(f)$ is the one-sided frequency wall-pressure ASD function and the factor 8
 78 accounts for pressure doubling at the panel surface [11]. The radiated power of the panel

79 into the receiving medium is obtained by integrating the normal active sound intensity flow
 80 passing through a virtual surface Σ_v surrounding the panel

$$\Pi_{rad}(f) = \iint_{\Sigma_v} \mathbf{I}_{act}(\mathbf{x}, f) \mathbf{n} d\mathbf{x}, \quad (3)$$

81 \mathbf{n} being the unit exterior vector normal to Σ_v , $d\mathbf{x}$ the surface element and $\mathbf{I}_{act}(\mathbf{x}, f)$ the
 82 active sound intensity at point \mathbf{x} . The latter is directly related to the one-sided frequency
 83 CSD function $G_{pv_0}(\mathbf{x}, f)$ between the sound pressure p and the particle velocity v_0 at point
 84 \mathbf{x} with [12]

$$\mathbf{I}_{act}(\mathbf{x}, f) = \text{Re}\{G_{pv_0}(\mathbf{x}, f)\}. \quad (4)$$

85 Theoretically, the radiated power is obtained by solving the formal integral in Eq. (3).
 86 For numerical and experimental applications, the integral of Eq. (3) may be approximated
 87 by discretizing the surface Σ_v and using the rectangular integration rule:

$$\Pi_{rad}(f) \approx \sum_{\mathbf{x} \in \sigma_v} \mathbf{I}_{act}(\mathbf{x}, f) \mathbf{n} \delta\mathbf{x}, \quad (5)$$

88 where σ_v represents the set of points defined on Σ_v and $\delta\mathbf{x}$ is the elementary point area.

89 To characterize the vibration response of a panel to a DAF, it is then necessary to
 90 evaluate G_{vv} at the considered point on the panel while the evaluation of G_{pv_0} for the set
 91 of points σ_v is required to estimate the TL. An approach for evaluating these quantities
 92 based on deterministic transfer functions and using a reciprocity principle is presented in
 93 the following sections.

94 **III. MATHEMATICAL FORMULATION OF THE VIBROACOUSTIC RESPONSE** 95 **OF PANELS UNDER DIFFUSE ACOUSTIC FIELD**

96 Let us consider the blocked wall-pressure field $p_b(\tilde{\mathbf{x}}, t)$ exerted on the panel by a DAF
 97 excitation at point $\tilde{\mathbf{x}}$ as a function of time. The response of the panel at point \mathbf{x} when the
 98 panel is excited by $p_b(\tilde{\mathbf{x}}, t)$ is denoted $\alpha(\mathbf{x}, t)$. If \mathbf{x} is on the panel, α stands for v whereas
 99 it stands for p or v_0 if \mathbf{x} is in the acoustic domain. This response can be expressed by the

100 convolution product [13]

$$\alpha(\mathbf{x}, t) = \iint_{\Sigma_p} \int_{-\infty}^{\infty} h_{\alpha/F_n}(\mathbf{x}, \tilde{\mathbf{x}}, t - \tau) p_b(\tilde{\mathbf{x}}, \tau) d\tau d\tilde{\mathbf{x}}, \quad (6)$$

101 where $h_{\alpha/F_n}(\mathbf{x}, \tilde{\mathbf{x}}, t)$ is the impulse response (structural velocity, acoustic pressure or particle
102 velocity-wise) at point \mathbf{x} for a normal unit force applied at point $\tilde{\mathbf{x}}$. Assuming that the
103 random process is ergodic, the cross-correlation function $R_{\alpha\alpha'}(\mathbf{x}, t)$ is defined by

$$R_{\alpha\alpha'}(\mathbf{x}, t) = \int_{-\infty}^{\infty} \alpha(\mathbf{x}, \tau) \alpha'(\mathbf{x}, t + \tau) d\tau. \quad (7)$$

104 where α' also designates v , p or v_0 . Introducing Eq. (6) in Eq. (7) and performing a time
105 Fourier transform of the resulting expression of the cross-correlation function gives the space-
106 frequency spectrum $S_{\alpha\alpha'}(\mathbf{x}, \omega)$, which after some manipulations (see [13] for details) can be
107 written as

$$S_{\alpha\alpha'}(\mathbf{x}, \omega) = \iint_{\Sigma_p} \iint_{\Sigma_p} H_{\alpha/F_n}(\mathbf{x}, \tilde{\mathbf{x}}, \omega) H_{\alpha'/F_n}^*(\mathbf{x}, \tilde{\mathbf{x}}, \omega) S_{p_b p_b}(\tilde{\mathbf{x}}, \tilde{\mathbf{x}}, \omega) d\tilde{\mathbf{x}} d\tilde{\mathbf{x}}, \quad (8)$$

108 where $H_{\alpha/F_n}(\mathbf{x}, \tilde{\mathbf{x}}, \omega)$ is the time Fourier transform of $h_{\alpha/F_n}(\mathbf{x}, \tilde{\mathbf{x}}, t)$ and corresponds to the
109 panel frequency response function (velocity, pressure or particle velocity-wise) at point \mathbf{x}
110 when it is excited by a normal force F_n applied at point $\tilde{\mathbf{x}}$; $S_{p_b p_b}(\tilde{\mathbf{x}}, \tilde{\mathbf{x}}, \omega)$ is the time
111 Fourier transform of the cross-correlation function of the blocked wall-pressure; finally * is
112 the complex conjugate. Defining the wavenumber-frequency spectrum of the wall-pressure
113 $S_{p_b p_b}(\mathbf{k}, \omega)$ as the wavenumber transform of the space-frequency spectrum $S_{p_b p_b}(\tilde{\mathbf{x}}, \tilde{\mathbf{x}}, \omega)$,
114 one has

$$S_{p_b p_b}(\tilde{\mathbf{x}}, \tilde{\mathbf{x}}, \omega) = \frac{1}{4\pi^2} \iint_{-\infty}^{\infty} S_{p_b p_b}(\mathbf{k}, \omega) e^{j\mathbf{k}(\tilde{\mathbf{x}} - \tilde{\mathbf{x}})} d\mathbf{k}. \quad (9)$$

115 where $\mathbf{k} = (k_x, k_y)$ is the wavevector defined in the plane (x, y) and $d\mathbf{k}$ is the two-dimensional
116 wavenumber element. By introducing Eq. (9) in Eq. (8) and rearranging the terms, one
117 obtains

$$S_{\alpha\alpha'}(\mathbf{x}, \omega) = \frac{1}{4\pi^2} \iint_{-\infty}^{\infty} H_{\alpha}(\mathbf{x}, \mathbf{k}, \omega) H_{\alpha'}^*(\mathbf{x}, \mathbf{k}, \omega) S_{p_b p_b}(\mathbf{k}, \omega) d\mathbf{k}, \quad (10)$$

118 where

$$H_{\alpha}(\mathbf{x}, \mathbf{k}, \omega) = \iint_{\Sigma_p} H_{\alpha/F_n}(\mathbf{x}, \tilde{\mathbf{x}}, \omega) e^{-j\mathbf{k}\tilde{\mathbf{x}}} d\tilde{\mathbf{x}}. \quad (11)$$

119 The $H_\alpha(\mathbf{x}, \mathbf{k}, \omega)$ functions are called the sensitivity functions [14] and characterize the vi-
 120 broacoustic behavior of the panel. The function $H_{\alpha/F_n}(\mathbf{x}, \tilde{\mathbf{x}}, \omega)$ is the time Fourier transform
 121 $h_{\alpha/F_n}(\mathbf{x}, \tilde{\mathbf{x}}, t)$ and, therefore, corresponds to the transfer function between the panel velocity
 122 frequency response and the frequency spectrum of the applied effort.

123 The wall-pressure CSD function in the space-frequency domain of a DAF can be expressed
 124 by [15]

$$S_{p_b p_b}(r, \omega) = S_{p_b p_b}(\omega) \frac{\sin(k_0 r)}{k_0 r}, \quad (12)$$

125 where $r = |\tilde{\mathbf{x}} - \tilde{\tilde{\mathbf{x}}}|$, $k_0 = \omega/c_0$ is the acoustic wavenumber and $S_{p_b p_b}(\omega)$ is the wall-pressure
 126 ASD function. The space-wavenumber transform of Eq. (12) gives the wall-pressure CSD
 127 function in the wavenumber-frequency space

$$S_{p_b p_b}(\mathbf{k}, \omega) = S_{p_b p_b}(\omega) \Phi_{p_b p_b}(\mathbf{k}, \omega), \quad (13)$$

128 where

$$\Phi_{p_b p_b}(\mathbf{k}, \omega) = \begin{cases} \frac{2\pi}{k_0} \frac{1}{\sqrt{k_0^2 - |\mathbf{k}|^2}} & \text{if } |\mathbf{k}| < k_0 \\ 0 & \text{if } |\mathbf{k}| \geq k_0 \end{cases}. \quad (14)$$

129 As the wall-pressure CSD function of a DAF is null for wavenumbers larger than the acoustic
 130 wavenumber, the integration domain involved in Eq. (10) can be restricted to the wavenum-
 131 bers contained in the acoustic domain (*i.e.*, $|\mathbf{k}| < k_0$). Moreover, in practice, this integral
 132 is approximated considering a set of wavevectors in the acoustic domain $\Omega_{\mathbf{k}}$ and using the
 133 rectangular integration rule. It should be stressed here that $S_{\alpha\alpha'}(\mathbf{x}, \omega)$ is a two-sided spec-
 134 trum as a function of the angular frequency. It can be related to the one-sided spectrum as
 135 a function of the frequency $G_{\alpha\alpha'}(\mathbf{x}, f)$ by

$$G_{\alpha\alpha'}(\mathbf{x}, f) = 4\pi S_{\alpha\alpha'}(\mathbf{x}, \omega). \quad (15)$$

136 For the sake of coherence with experiments, one-sided frequency spectra will be considered
 137 in the remainder of the article.

138 According to Eq. (10) and (15), the one-sided frequency ASD function of the velocity v

139 at point \mathbf{x} ($z = 0$) of a panel excited by a DAF can be estimated with

$$G_{vv}(\mathbf{x}, f) \approx \frac{1}{4\pi^2} \sum_{\mathbf{k} \in \Omega_{\mathbf{k}}} |H_v(\mathbf{x}, \mathbf{k}, \omega)|^2 G_{p_b p_b}(f) \Phi_{p_b p_b}(\mathbf{k}, \omega) \delta^2 \mathbf{k}, \quad (16)$$

140 whereas the one-sided frequency CSD function between the pressure p and the particle
141 velocity v_0 at a given point \mathbf{x} into the acoustic domain can be estimated with

$$G_{pv_0}(\mathbf{x}, f) \approx \frac{1}{4\pi^2} \sum_{\mathbf{k} \in \Omega_{\mathbf{k}}} H_p(\mathbf{x}, \mathbf{k}, \omega) H_{v_0}^*(\mathbf{x}, \mathbf{k}, \omega) G_{p_b p_b}(f) \Phi_{p_b p_b}(\mathbf{k}, \omega) \delta^2 \mathbf{k}, \quad (17)$$

142 where $\delta \mathbf{k}$ represents the wavenumber resolution and $G_{p_b p_b}(f) = 4\pi S_{p_b p_b}(\omega)$ is the one-sided
143 frequency ASD function of the blocked wall-pressure.

144 To evaluate these two quantities, the sensitivity functions H_v , H_p and H_{v_0} for wavenum-
145 bers belonging to $\Omega_{\mathbf{k}}$ are thus to be determined. A direct interpretation of these sensitivity
146 functions can be deduced from Eq. (11). Since $H_{\alpha/F_n}(\mathbf{x}, \tilde{\mathbf{x}}, \omega)$ is the response α at point \mathbf{x}
147 for a unit normal force at point $\tilde{\mathbf{x}}$, H_{α} represents the frequency response α at point \mathbf{x} due
148 to a wall-pressure plane wave of wavevector $-\mathbf{k}$ (*i.e.*, due to the pressure field $e^{-j\mathbf{k}\tilde{\mathbf{x}}}$). This
149 direct interpretation is depicted in Figs. 2(a), 2(c) and 2(e) for H_v , H_p and H_{v_0} , respectively.

150 The sensitivity functions must, therefore, be estimated only at the point of interest \mathbf{x}
151 and for the set of wavevectors $\Omega_{\mathbf{k}}$. A large number of waves should be considered to entirely
152 cover the acoustic wavenumber domain. Moreover, from an experimental point of view,
153 wall-pressure plane waves cannot be easily reproduced. To circumvent these issues, another
154 interpretation of these sensitivity functions based on the reciprocity principle is given in the
155 next section.

156 IV. ALTERNATIVE INTERPRETATION OF THE SENSITIVITY FUNCTIONS

157 In order to propose another interpretation of the sensitivity functions, let us consider the
158 standard reciprocity principle which states that the response of a system is invariant with
159 respect to the exchange of points of excitation and observed response [16]. Following the
160 previous notation, it can be translated into

$$H_{\alpha/F_n}(\mathbf{x}, \tilde{\mathbf{x}}, \omega) = H_{v/\tilde{\alpha}}(\tilde{\mathbf{x}}, \mathbf{x}, \omega), \quad (18)$$

161 where $H_{v/\bar{\alpha}}(\tilde{\mathbf{x}}, \mathbf{x}, \omega)$ is the frequency response function between the panel velocity and a
 162 source $\bar{\alpha}$, dual of α . As the normal force F_n is applied on the panel, the exchanged observa-
 163 tion point is also on the panel which explains why the right-hand side of Eq. (18) remains
 164 the velocity response of the panel, regardless of α . However the type of excitation source $\bar{\alpha}$
 165 depends on α and it will be detailed below for each quantity considered for α .

166 Sticking to the general case, by introducing Eq. (18) in Eq. (11) one obtains

$$H_{\alpha}(\mathbf{x}, \mathbf{k}, \omega) = \iint_{\Sigma_p} H_{v/\bar{\alpha}}(\tilde{\mathbf{x}}, \mathbf{x}, \omega) e^{-j\mathbf{k}\tilde{\mathbf{x}}} d\tilde{\mathbf{x}}. \quad (19)$$

167 The right hand side of Eq. (19) can be interpreted as the space-wavenumber transform of
 168 $H_{v/\bar{\alpha}}(\tilde{\mathbf{x}}, \mathbf{x}, \omega)$ with respect to the spatial variable $\tilde{\mathbf{x}}$. The points $\tilde{\mathbf{x}}$ become observation points
 169 on the panel surface Σ_p , which means that the space-wavenumber transform is performed
 170 over the vibration velocity field of the panel. To sum up, the sensitivity function $H_{\alpha}(\mathbf{x}, \mathbf{k}, \omega)$
 171 may be obtained by exciting the panel with a source $\bar{\alpha}$ at point \mathbf{x} and by calculating the
 172 space-wavenumber transform of the panel velocity frequency response normalized by the
 173 source frequency spectrum. This second interpretation of the sensitivity functions is now
 174 detailed for the three cases involved in the evaluation of the panel response excited by a
 175 DAF.

176 **Case of plate velocity** ($\alpha = v$): The reciprocity principle states [17] that the ratio of
 177 the normal velocity of the panel at point \mathbf{x} over the applied normal force at point $\tilde{\mathbf{x}}$ is equal
 178 to the ratio of the normal velocity of the panel at point $\tilde{\mathbf{x}}$ over the normal force applied at
 179 point \mathbf{x} . Eq. (18) becomes

$$H_{v/F_n}(\mathbf{x}, \tilde{\mathbf{x}}, \omega) = H_{v/F_n}(\tilde{\mathbf{x}}, \mathbf{x}, \omega). \quad (20)$$

180 In this case, $\bar{\alpha}$ is a normal force and thus, the sensitivity function $H_v(\mathbf{x}, \mathbf{k}, \omega)$ is obtained
 181 by exciting the panel with a normal force at point \mathbf{x} and by performing a space-wavenumber
 182 transform of the transfer function between the panel vibration velocity response and the
 183 force frequency spectrum, as illustrated in Fig. 2(b).

184 **Case of radiated pressure** ($\alpha = p$): Lyamshev reciprocity relations for elastic struc-
 185 tures excited by point forces [16] indicate that the ratio of the pressure at point \mathbf{x} over the
 186 applied normal force at point $\tilde{\mathbf{x}}$ is equal to the ratio of the normal velocity of the panel at

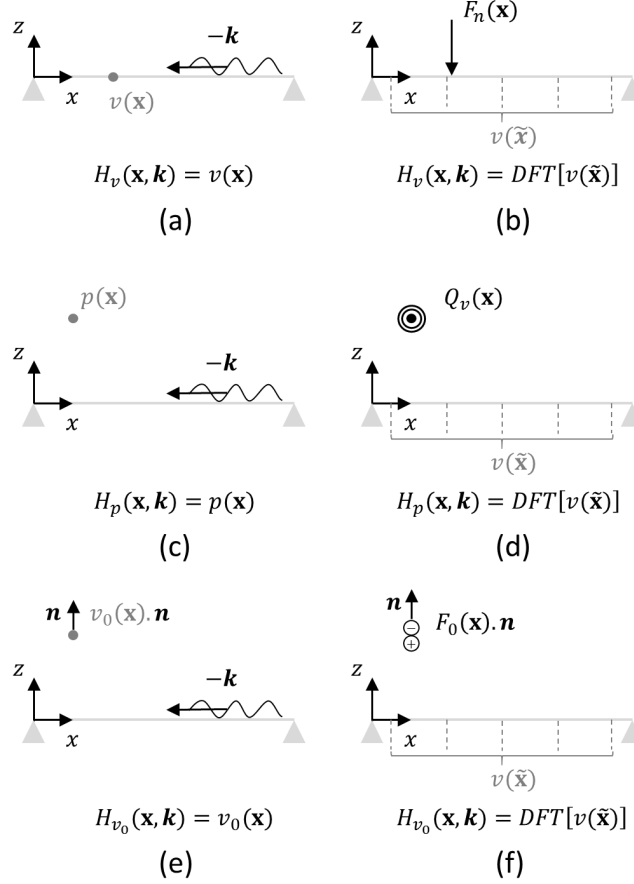


FIG. 2. Direct interpretation of the sensitivity functions: (a) H_v , (c) H_p , (e) H_{v_0} and corresponding reciprocal interpretation (b) H_v , (d) H_p , (f) H_{v_0} . (d) and (f) see appendix for demonstration.

187 point $\tilde{\mathbf{x}}$ over the volume velocity Q_v of a monopole source placed at point \mathbf{x} . The demon-
 188 stration of this particular reciprocity relation according to Lyamshev [18] is provided in
 189 Appendix A 1 (this classical demonstration is useful to introduce reciprocity in terms of
 190 particle velocity and dipole source strength, which is demonstrated in appendix A 2). In
 191 this case $\bar{\alpha}$ is a monopole source of volume velocity Q_v and Eq. (18) becomes

$$H_{p/F_n}(\mathbf{x}, \tilde{\mathbf{x}}, \omega) = H_{v/Q_v}(\tilde{\mathbf{x}}, \mathbf{x}, \omega). \quad (21)$$

192 The sensitivity function $H_p(\mathbf{x}, \mathbf{k}, \omega)$ is therefore obtained by exciting the panel with a
 193 monopole source at point \mathbf{x} and by performing a space-wavenumber transform of the panel
 194 vibration velocity response normalized by the frequency spectrum of the monopole's volume
 195 velocity, as illustrated in Fig. 2(d).

196 **Case of particle velocity** ($\alpha = v_0$): Fahy stated that the reciprocity relationship could
 197 be extended to acoustic dipoles and particle velocities [16], however no demonstration could
 198 be found in the literature. As a point dipole can be represented by a point force injected in
 199 the fluid, the ratio of the particle velocity at point \mathbf{x} over the applied normal force at point
 200 $\tilde{\mathbf{x}}$ is equal to the ratio of the normal velocity of the panel at point $\tilde{\mathbf{x}}$ over the force injected
 201 in the fluid F_0 at point \mathbf{x} . This latter reciprocity relation is demonstrated in Appendix A 2.
 202 The dual source $\bar{\alpha}$ being a dipole source of force F_0 injected in the fluid, Eq. (18) now
 203 becomes

$$H_{v_0/F_n}(\mathbf{x}, \tilde{\mathbf{x}}, \omega) = H_{v/F_0}(\tilde{\mathbf{x}}, \mathbf{x}, \omega) \quad (22)$$

204 As demonstrated in Appendix A 2, the force F_0 is injected in the same direction \mathbf{n} as
 205 the desired direction of the particle velocity v_0 . One can obtain the sensitivity function
 206 $H_{v_0}(\mathbf{x}, \mathbf{k}, \omega)$ by exciting the panel with a dipole source at point \mathbf{x} and by performing a
 207 space-wavenumber transform of the panel vibration velocity response normalized by the
 208 frequency spectrum of the force injected by the dipole source in the fluid, as illustrated in
 209 Fig. 2(f).

210 To sum up, the sensitivity functions can be obtained by exciting the system at the point
 211 of interest \mathbf{x} and by performing a space-wavenumber transform of the panel velocity field.
 212 In practice, the vibratory field has to be measured on a regular grid of points denoted
 213 $\Gamma_{\tilde{\mathbf{x}}}$, using a scanning laser vibrometer, for example. The space-wavenumber transform is
 214 therefore approximated by a discrete Fourier transform. In order to avoid aliasing effects,
 215 the spatial resolution $\delta\tilde{\mathbf{x}}$ over $\Gamma_{\tilde{\mathbf{x}}}$ should be determined so that the spatial variations of
 216 the vibratory field can be correctly represented by the grid of points. For a homogeneous
 217 isotropic thin panel, $\delta\tilde{\mathbf{x}}$ should be less than or equal to a quarter of the natural flexural
 218 wavelength of the panel λ_f at the highest frequency of interest. For a more complex panel,
 219 a preliminary study should be carried out to define this parameter (for instance, by using a
 220 numerical model of the panel or by using a trial and error procedure).

221 V. DESCRIPTION OF THE PROPOSED METHODOLOGY

222 A methodology for experimentally estimating the vibroacoustic response of a panel excited
 223 by a DAF is now presented. This methodology is based on Eqs. (16) and (17), and the second
 224 interpretation of the sensitivity functions, as described in the previous section.

225 **Vibration response of the panel:** The methodology for evaluating the velocity ASD
 226 function G_{vv} at a given point \mathbf{x} of the panel ($z = 0$) can be summarized as follows:

- 227 - Excite the panel with a normal mechanical force at point \mathbf{x} (for instance by using a
 228 shaker) and measure the normal velocity response of the panel at points $\tilde{\mathbf{x}} \in \Gamma_{\tilde{\mathbf{x}}}$ to
 229 determine $H_{v/F_n}(\tilde{\mathbf{x}}, \mathbf{x}, \omega)$,
- 230 - Perform a discrete Fourier transform of the panel velocity response $H_{v/F_n}(\tilde{\mathbf{x}}, \mathbf{x}, \omega)$
 231 (with respect to $\tilde{\mathbf{x}}$) to obtain the sensitivity functions $H_v(\mathbf{x}, \mathbf{k}, \omega)$ at point \mathbf{x} for $\mathbf{k} \in \Omega_{\mathbf{k}}$,
- 232 - Use Eqs. (16) and (14) to estimate the velocity ASD function G_{vv} at point \mathbf{x} under an
 233 ideal DAF excitation.

234 **Acoustic response of the panel:** The acoustic response of the panel is characterized
 235 by the TL as described in Sec. II. It can be obtained by following the next five steps:

- 236 - Excite the panel with a monopole source at a given point of interest \mathbf{x} and measure the
 237 normal velocity response of the panel at points $\tilde{\mathbf{x}} \in \Gamma_{\tilde{\mathbf{x}}}$ to determine $H_{v/Q_v}(\tilde{\mathbf{x}}, \mathbf{x}, \omega)$,
- 238 - Excite the panel with a dipole source at a given point of interest \mathbf{x} and measure the
 239 normal velocity response of the panel at points $\tilde{\mathbf{x}} \in \Gamma_{\tilde{\mathbf{x}}}$ to determine $H_{v/F_0}(\tilde{\mathbf{x}}, \mathbf{x}, \omega)$,
- 240 - Perform a discrete Fourier transform of the panel velocity responses obtained for
 241 both monopole and dipole cases to estimate the sensitivity functions $H_p(\mathbf{x}, \mathbf{k}, \omega)$ and
 242 $H_{v_0}(\mathbf{x}, \mathbf{k}, \omega)$ at point \mathbf{x} ,
- 243 - Calculate the pressure – particle velocity CSD function at point \mathbf{x} using Eqs. (17)
 244 and (14),
- 245 - Calculate the active sound intensity at point \mathbf{x} using Eq. (4).

246 The five previous steps are repeated for points $\mathbf{x} \in \sigma_v$ (discretizing the whole virtual
 247 surface Σ_v surrounding the panel) to calculate the radiated power using Eq. (5). The TL is
 248 finally deduced using Eq. (1) while the incident acoustic power is evaluated with Eq. (2).

249 **VI. NUMERICAL AND EXPERIMENTAL VALIDATION OF THE PROPOSED**
 250 **APPROACH**

251 **A. Test case description**

252 For numerical and experimental validation purposes a test case is considered, which
 253 consists in a rectangular thin aluminum plate, simply supported on its four edges, baffled,
 254 and submitted to a DAF excitation on one side. This baffled plate separates two semi-infinite
 255 domains filled with air ($\rho_0 = 1.3 \text{ kg.m}^{-3}$ and $c_0 = 343 \text{ m.s}^{-1}$). The plate's geometrical and
 256 mechanical properties are detailed in Table I. The structural loss factor η_{mn} of the (m, n)
 257 mode has been experimentally estimated using the -3 dB bandwidth method on the first
 258 few resonances of the plate and is taken into account in the numerical simulations. A mean
 259 value of $\eta = 0.005$ has been measured. Simply-supported boundary conditions have been
 260 chosen because they lead to a simple analytical solution of the plate equation of motion.
 261 In addition, the experimental setup proposed by Robin et al. [19] for reproducing these
 262 boundary conditions has already been validated.

263 The frequency range of interest is [170, 2000 Hz] with a frequency resolution of 0.625 Hz.
 264 The low frequency limit is set according to the frequency response of the monopole source
 265 and the high frequency limit has been chosen arbitrarily. This frequency range is below the
 266 critical frequency of the panel, f_c , given by

$$f_c = \frac{c_0^2}{2\pi} \sqrt{\frac{\rho h}{D}}, \quad (23)$$

267 where $D = \frac{Eh^3}{12(1-\nu^2)}$ is the flexural stiffness. For the considered case, $f_c = 3867 \text{ Hz}$.

268 In this section, we will focus on:

- 269 - the velocity sensitivity functions H_v at point \mathbf{x}_M of coordinates $(x = 0.06 \text{ m}, y = 0.3 \text{ m}, z = 0 \text{ m})$
 270 on the plate,
- 271 - the pressure and particle velocity sensitivity functions H_p and H_{v_0} at point \mathbf{x}_N of
 272 coordinates $(x = 0.06 \text{ m}, y = 0.3 \text{ m}, z = 0.1 \text{ m})$ into the acoustic medium. The particle
 273 velocity v_0 will be determined in direction z ,
- 274 - the frequency response of the velocity response at point \mathbf{x}_M and of the active intensity
 275 at point \mathbf{x}_N in the direction z .

276 To apply the methodology described in Sec. V, the panel velocity field has to be measured
 277 or calculated on a grid of points $\Gamma_{\tilde{\mathbf{x}}}$. In the following, a uniform mesh of 15×13 points is
 278 considered in directions x and y respectively and a gap of 30 mm along the edges is left for
 279 practical reasons. This leads to a spatial resolution of $\delta_x = \delta_y = 30$ mm and ensures at least
 280 4 points per flexural wavelength for all frequencies of interest. The highest wavenumbers
 281 k_x^{max} and k_y^{max} that can be resolved in directions x and y , respectively, are given by

$$k_x^{max} = k_y^{max} = \frac{\pi}{\delta_x} = \frac{\pi}{\delta_y} \simeq 105 \text{ m}^{-1}. \quad (24)$$

282 These wavenumbers are well above twice the acoustic wavenumber (related to the Shan-
 283 non criterion) at the highest frequency of interest (*i.e.*, $k_0 = 37 \text{ m}^{-1}$ at 2000 Hz). As
 284 a consequence, the considered grid of points provides correct estimation of the sensitivity
 285 functions in the acoustic wavenumber domain $\Omega_{\mathbf{k}}$. The wavenumber resolutions δk_x and δk_y
 286 in directions x and y respectively, are given by

$$\delta k_x = \frac{2\pi}{L_x} \simeq 13 \text{ m}^{-1}; \quad \delta k_y = \frac{2\pi}{L_y} \simeq 15 \text{ m}^{-1}. \quad (25)$$

287 These wavenumber resolutions are relatively large because of the small dimensions of the
 288 panel. In order to improve the wavenumber resolution, zero-padding is used to obtain a
 289 wavenumber resolution of 0.5 m^{-1} along k_x and k_y .

290 In order to assess the accuracy of the reciprocity approach for evaluating the panel sensi-
 291 tivity functions, the results obtained with this approach are compared with those obtained
 292 by considering the direct interpretation of these functions (as described in Sec. III). This
 293 comparison will allow validating the uniform mesh of 15×13 points used for the discrete
 294 spatial Fourier transform of the panel velocity field. The numerical model used for this study
 295 is described in Appendix B.

296 B. Experimental set-up

297 Fig. 3 shows the experimental setup used to measure the sensitivity functions. The
 298 plate was glued on thin blades and fixed on a frame as described in [19] to reproduce simply

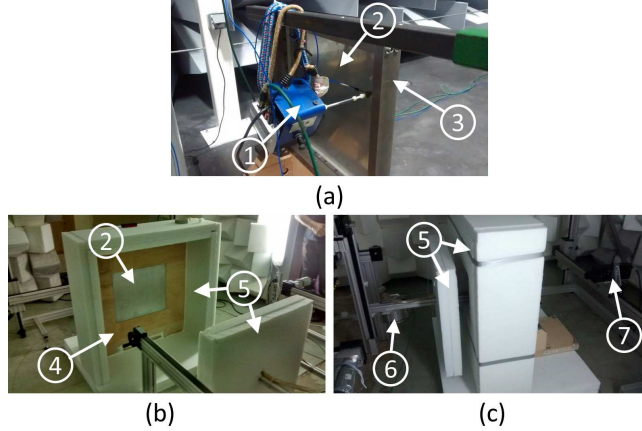


FIG. 3. Experimental setup. (a) plate excited by a shaker to determine H_v . (b) and (c) baffled plate excited by a monopole source to determine H_p and H_{v_0} . 1 - shaker with impedance head. 2 - plate. 3 - frame. 4 - baffle. 5 - sound absorbing foam. 6 - monopole source mounted on 3-axis robot. 7 - single-point laser vibrometer mounted on 2-axis robot.

299 supported boundary conditions. To determine the velocity sensitivity functions H_v , the plate
 300 was excited by a normal force at point \mathbf{x}_M of coordinates ($x = 0.06$ m, $y = 0.3$ m, $z = 0$ m).
 301 This force was applied using a TMS SmartShaker K2007E01 with integrated amplifier, which
 302 was fed with a swept sine over the considered frequency range and the force was measured
 303 using an impedance head PCB288D01 (as shown in Fig. 3(a)). An adapter was used between
 304 the impedance head and the plate reducing the area of mechanical coupling to approximately
 305 a 5 mm diameter circle.

306 For acoustic applications, the plate was baffled in a 1×1 m² plywood panel of 2 cm
 307 thickness. The experiment was performed in a hemi-anechoic room and 10 cm thick sound
 308 absorbing foam (Decibel France Polyphone 63 T) was placed on the ground and around the
 309 plate (see Figs. 3(b) and 3(c)) to avoid potential reflections and possible influence of the
 310 background noise generated by the robot used to estimate the TL (see Figs. 3(c) and section
 311 VII B). This allowed approaching fully anechoic conditions and ideal monopole and dipole
 312 excitations.

313 To estimate the pressure sensitivity functions at point \mathbf{x}_N of coordinates ($x = 0.06$ m, $y =$
 314 0.3 m, $z = 0.1$ m), the plate was excited by a Microflown Mid-High frequency monopole-
 315 HFM source at point \mathbf{x}_N fed with a white noise signal on the considered frequency range.
 316 The monopole source consists of a high impedance loudspeaker connected to a socket by a
 317 tube with an inner diameter of 15 mm. The frequency range over which the source is effective

318 and acts like a monopole is [100, 7000 Hz]. The calibration of the source (volume velocity
319 Q_v per unit input voltage U) was obtained by measuring the radiated sound pressure p at a
320 given distance r in anechoic conditions for a given input voltage U and using the theoretical
321 model of a monopole in free field for the relation between p and Q_v . The effect of the tube
322 on the frequency response has thereby been accounted for.

323 To estimate the particle velocity sensitivity functions at point \mathbf{x}_N in the direction z ,
324 the response of the plate to a dipole source has been reconstructed by exciting the plate
325 with the same monopole source, still fed with a white signal and moved from the previous
326 position by a distance $d = 3$ cm in the direction of the injected force (in this case z).
327 Two monopoles close to each other and out of phase have been thereby reconstructed by
328 subtracting the measured transfer functions H_v/Q_v . A preliminary experimental study in free
329 field conditions and using the plate was performed to determine an appropriate separation d .
330 It showed that below a separation of 0.5 cm, the vibration fields induced for both positions
331 of the monopole source were not sufficiently different to be noticeably measured. On the
332 other hand, above a separation of 5 cm, the directivity of the reconstructed dipole did not
333 match that of a theoretical dipole. A value of 3 cm for d appeared to be an optimal value
334 for the present case. It should be noted that the condition $k_0 d \ll 1$ does not hold at the
335 highest frequencies. However, the induced vibrations were in accordance with the response
336 of a plate to a theoretical dipole. Since the numerical and experimental sensitivity functions
337 and pressure - particle velocity CSD functions are in good agreement (see next section),
338 these results validate the experimental method for reconstructing a dipole source.

339 According to the methodology described in Sec. V, the vibratory response of the panel
340 has been measured on the grid of 15×13 points with a single point Polytec laser vibrometer
341 for each case of the excitation (*i.e.*, force, monopole, dipole). Also, in each case, the time
342 Fourier transform was directly performed in the post-processing software with ten linear
343 averages.

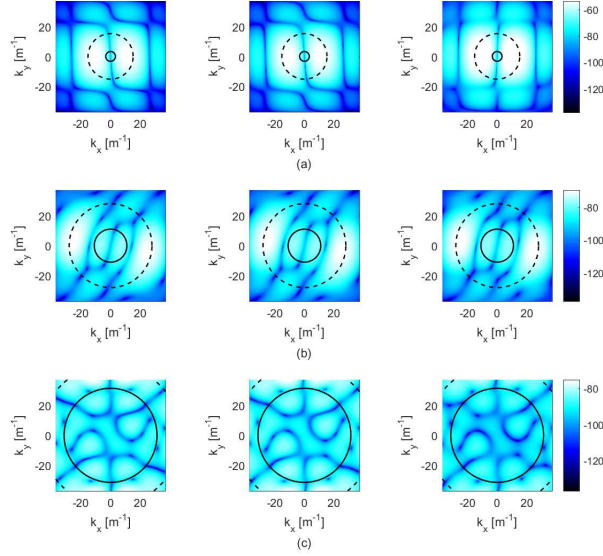


FIG. 4. Velocity sensitivity functions at point \mathbf{x}_M , $|H_v|^2$ (dB, ref. $1 \text{ m}^2 \cdot \text{s}^{-2}$): direct calculation (left), numerical reciprocity approach (middle), experimental reciprocity approach (right). (a) $f = 178$ Hz. (b) $f = 600$ Hz. (c) $f = 1710$ Hz. - - -, circle of radius k_f . —, circle of radius k_0 .

344 C. Comparison between numerical and experimental results

345 1. Sensitivity functions

346 Fig. 4 shows the velocity sensitivity functions H_v obtained with the direct calculation
 347 and the reciprocal approach using numerical and experimental data, respectively. They are
 348 provided for three different frequencies, the lowest corresponding to the (2,1) vibration mode
 349 frequency (Fig. 4(a)) and the two others being off-resonance cases (Figs. 4(b) and 4(c)).
 350 The product of sensitivity functions H_p and $H_{v_0}^*$, which is involved in the expression of
 351 G_{pv_0} (Eq. (17)), is shown in Fig. 5 at the same frequencies. The circles of radius k_0 and
 352 $k_f = \sqrt{\frac{2\pi f c}{c_0}} k_0$, corresponding to the acoustic and flexural natural wavenumbers respectively,
 353 are also indicated in Figs. 4 and 5.

354 In Fig. 4 and 5, results obtained by simulating numerically the direct and the reciprocity
 355 methods match perfectly. This validates the grid of points considered on the panel and
 356 the use of zero-padding to improve the wavenumber resolution without affecting the results.
 357 It also validates the method described above to reconstruct a dipole from two monopole
 358 sources.

359 In Fig. 4 and 5, the numerical and experimental results are generally in good agreement.

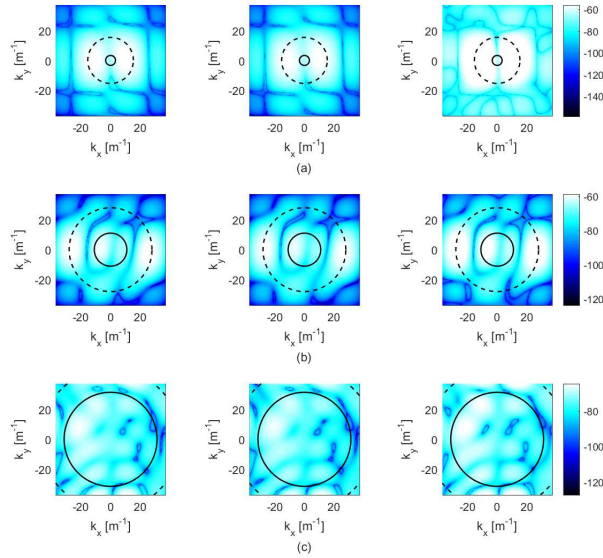


FIG. 5. Product of sensitivity functions at point \mathbf{x}_N , $|\text{Re}\{H_p \times H_{v_0}^*\}|$ (dB, ref. $1 \text{ Pa}\cdot\text{m}\cdot\text{s}^{-1}$): direct calculation (left), numerical reciprocity approach (middle), experimental reciprocity approach (right). (a) $f = 178$ Hz. (b) $f = 600$ Hz. (c) $f = 1710$ Hz. - - -, circle of radius k_f . —, circle of radius k_0 .

360 One can observe that the sensitivity functions are slightly overestimated experimentally at
 361 the (2,1) vibration mode frequency compared to the numerical results. This can be explained
 362 by the fact that the modal damping loss factor has been estimated from the response of the
 363 plate to a shaker excitation. The added mass from the shaker possibly had an influence on
 364 the evaluation of the damping of the (2,1) mode.

365 A good agreement is particularly noticed within the acoustic wavenumber circle (delin-
 366 eated by a full line). Again, only values in the acoustic wavenumber domain contribute
 367 to the plate's vibroacoustic response to a DAF. However, the sensitivity functions are also
 368 correctly estimated experimentally for wavenumbers higher than the acoustic wavenumber.

369 2. Plate velocity ASD function

370 The velocity ASD function $G_{vv}(\mathbf{x}, f)$ at point \mathbf{x}_M of the panel excited by a DAF with a
 371 unit wall-pressure ASD function ($G_{p_b p_b}(f) = 1 \text{ Pa}^2\cdot\text{Hz}^{-1}$) has been estimated using Eq. (16)
 372 and the three previously described sensitivity functions. Fig. 6(a) compares the results
 373 obtained with the direct calculation and the numerical reciprocity approach. The two curves
 374 are perfectly superimposed, showing that the sensitivity functions obtained with the two

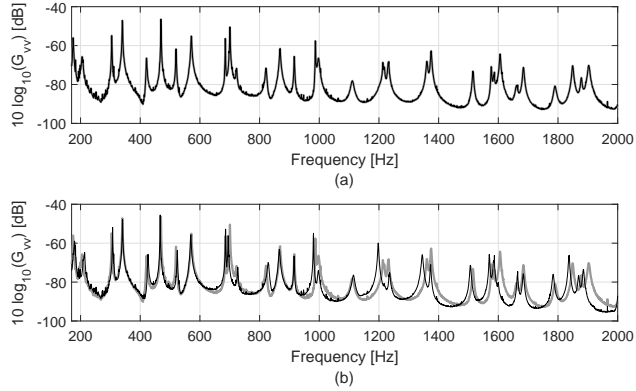


FIG. 6. Velocity ASD functions G_{vv} (dB, ref. $1 \text{ m}^2 \cdot \text{s}^{-2} \cdot \text{Hz}^{-1}$). (a) direct calculation (bold gray line) vs. numerical reciprocity approach (light black line). (b) numerical reciprocity approach (bold gray line) vs. experimental reciprocity approach (light black line).

375 approaches are essentially identical in the acoustic domain and on the whole considered
 376 frequency range. The small noticeable peaks between resonance frequencies of the plate on
 377 both curves are attributable to the wavenumber sampling in Eq. (16) which induces errors
 378 especially as $|\mathbf{k}|$ approaches k_0 , in which case the DAF wall-pressure CSD goes to infinity
 379 (see Eq. (14)).

380 Fig. 6(b) compares the results obtained numerically and experimentally while considering
 381 the reciprocity method to estimate the sensitivity functions. A good agreement is observed
 382 between the two results, which experimentally validates the proposed methodology for the
 383 considered test case. Slight shifts of the resonance peaks in the high frequency range are
 384 noticed. They can be explained by small differences between the experimental and the
 385 theoretical boundary conditions of the panel or more likely by the added mass from the
 386 shaker.

387 3. Pressure – particle velocity CSD function

388 Fig. 7(a) shows the real part of the pressure – particle velocity CSD function $G_{pv_0}(\mathbf{x}, f)$
 389 at point \mathbf{x}_N when the plate is excited by a DAF ($G_{p_b p_b}(f) = 1 \text{ Pa}^2 \cdot \text{Hz}^{-1}$). These results have
 390 been obtained using the direct calculation and the reciprocal approach for the sensitivity
 391 functions. Again, the two curves are in good agreement, which shows that the sensitivity
 392 functions H_p and H_{v_0} are properly determined on the entire frequency range using the

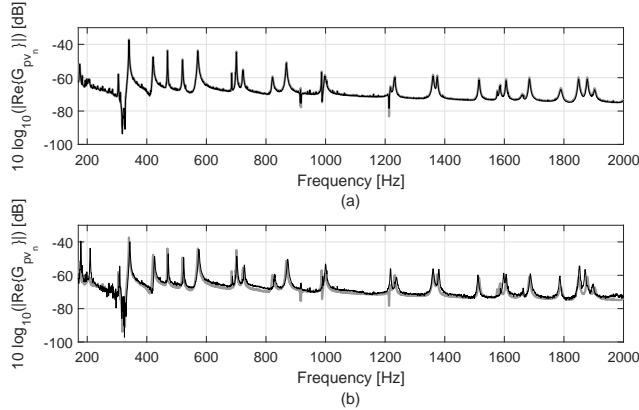


FIG. 7. Pressure – particle velocity CSD functions $\text{Re}\{G_{pv_0}\}$ (dB, ref. $1 \text{ W}^2 \cdot \text{m}^{-2} \cdot \text{Hz}^{-1}$). (a) direct calculation (bold gray line) vs. numerical reciprocity approach (light black line). (b) numerical reciprocity approach (bold gray line) vs. experimental reciprocity approach (light black line).

393 reciprocity principle.

394 The experimental and theoretical pressure – particle velocity CSD functions are com-
 395 pared in Fig. 7(b). Their good agreement shows that the active sound intensity is correctly
 396 estimated in this situation using the reciprocity approach. Furthermore, the experimental
 397 monopole and dipole excitations correctly reproduce the theoretical conditions. The reso-
 398 nance peaks are better estimated compared to those obtained to estimate the plate’s velocity
 399 ASD function in Fig. 6(b), particularly at high frequencies. This can be possibly explained
 400 by the accuracy in positioning the source which, for the experiment with the shaker was done
 401 manually (subject to more errors) whereas for the acoustic applications, it was controlled
 402 with a robot allowing a higher accuracy. A more likely explanation is the dynamic influence
 403 of the mass added with the shaker, which explains the slight shifts of the resonance peaks
 404 in Fig. 6(b).

405 VII. COMPARISON WITH REVERBERANT ROOM MEASUREMENTS

406 The proposed approach is finally compared with measurements performed at the Univer-
 407 sity of Sherbrooke transmission loss facility (coupled reverberant-anechoic rooms) using a
 408 plate similar to the one used in the previous section (similar dimensions, material and bound-
 409 ary conditions) and following test standard ASTM E2249-02 (2016) [4]. The reverberant
 410 room has a volume of approximately 140 m^3 ($7.5 \times 6.2 \times 3 \text{ m}^3$), and the Schroeder frequency

411 of the room, above which the sound field can be considered diffuse, is approximately 410 Hz.
 412 The plate was mounted in an existing niche between the coupled anechoic-reverberant rooms
 413 (the panel being flush mounted on the reverberant room side). A double-wall structure with
 414 mechanical decoupling was then built around the plate to prevent acoustic leaks and flank-
 415 ing paths, as described in [19]. A loudspeaker fed with a white noise signal excited the
 416 reverberant chamber.

417 **A. Panel velocity response**

418 A first experiment in the transmission loss facility was carried out to evaluate the vibra-
 419 tory response of the panel under a DAF. A Polytec scanning laser vibrometer placed on the
 420 anechoic side was used to measure the plate velocity ASD function. A 9×9 microphones
 421 array (1/4 inch B&K 4957) separated by 10 cm in directions x and y was centered to the
 422 plate and used to directly measure wall-pressure fluctuations 1 cm away from the plate. An
 423 average sound pressure level over all 81 microphones was then calculated to evaluate a mean
 424 wall-pressure ASD function $\bar{G}_{p_b p_b}(f)$ on the reverberant side.

425 The sensitivity functions of this second plate were estimated experimentally using the
 426 reciprocity method. Some differences with the sensitivity functions of the plate considered
 427 in Sec. VI (not shown here) indicate that the positioning of the force applied with the shaker
 428 is not exactly at the considered point \mathbf{x}_M . Indeed, the position has a significant influence
 429 on the vibratory response, particularly at high frequencies where the mode shapes get more
 430 complex. The mounting base of the force sensors also has a finite diameter of approximately
 431 5 mm, which makes the applied force not perfectly punctual. However, the modal frequencies
 432 correspond to the theory for both plates. The velocity ASD function was calculated using
 433 Eq. (16) and (14) whilst including the measured wall-pressure ASD function $\bar{G}_{p_b p_b}(f)$.

434 The plate velocity ASD function measured in the reverberant room at point \mathbf{x}_M is com-
 435 pared to the result obtained with the proposed method in Fig. 8. The two obtained responses
 436 are in good agreement up to 800 Hz. Above this frequency, differences are noticeable and
 437 can be explained with:

- 438 - the inaccuracy in the positioning of point \mathbf{x}_M where the velocity ASD function is
- 439 measured in the reverberant chamber (corresponding to the point force position in the
- 440 reciprocity method) whose influence increases with the frequency,

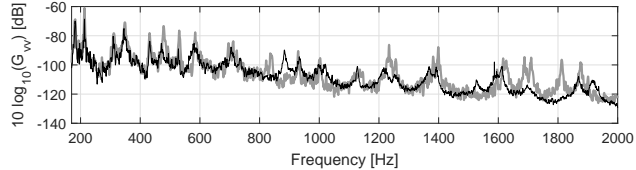


FIG. 8. Velocity ASD functions G_{vv} (dB, ref. $1 \text{ m}^2 \cdot \text{s}^{-2} \cdot \text{Hz}^{-1}$): reverberant room measurements (bold gray line) vs. experimental reciprocity approach (light black line).

441 - the deviation of the pressure field in reverberant room to an ideal DAF. An analysis
 442 of the pressure field measured with the microphone array shows spatial variations in
 443 contradiction with the assumptions of a perfect DAF. Moreover, it is well known that
 444 a reverberant chamber has difficulty creating grazing incidence waves. The absence
 445 of grazing incidence waves can hardly be quantified as it varies from one reverberant
 446 room to another. Some authors suggest corrections on the theoretical model of the
 447 excitation to better represent the actual excitation in a reverberant room [20] [21].

448 B. Sound transmission loss

449 A second experiment in the transmission loss facility was conducted for estimating the
 450 plate TL. A 1/2 inch Bruel & Kjaer rotating microphone was used to measure the spatially-
 451 averaged sound pressure level L_p in far radiation field. The average sound intensity level L_I
 452 was measured on the anechoic side by using a Bruel & Kjaer sound intensity probe composed
 453 of two 1/2 inch microphones with a 12 mm spacing. The sound intensity probe was manually
 454 moved 5 cm away from the plate to scan over a parallel surface identical to the plate area,
 455 as described in [4] for the case of a plate flush mounted on the source side. The transmission
 456 loss of the structure is given by $TL = L_p - L_I - 6$ [22]. An illustration of this experiment
 457 and the considered virtual surface is given in Fig. 9(a).

458 In addition, the proposed methodology described in Sec. V for estimating the TL was
 459 applied. A numerical study on the definition of the virtual surface Σ_v (which is not detailed
 460 in this paper) showed that considering a virtual surface equal to the plate area and positioned
 461 5 cm away from it would result in a slight overestimation of the TL, particularly at high
 462 frequencies. This overestimation is due to sound intensity levels outside the virtual surface
 463 Σ_v that are thus not taken into account in the calculation of the radiated power. The

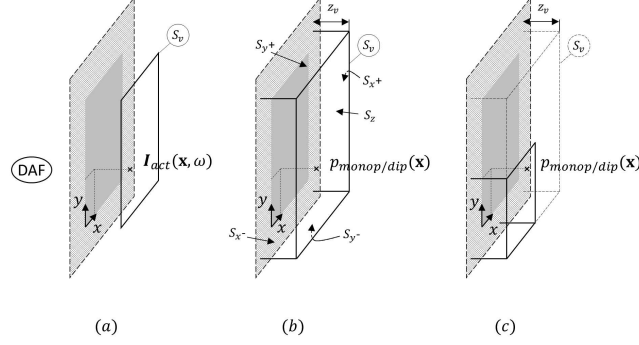


FIG. 9. Illustration of the virtual surface Σ_v considered for estimating the radiated power. (a) in the transmission loss facility. (b) with the reciprocal approach. (c) with the reciprocal approach considering the symmetry properties of the system.

464 virtual surface Σ_v over which the active sound intensity should be estimated to obtain the
 465 radiated power should enclose the plate entirely. Therefore, the considered surface Σ_v was
 466 decomposed into 5 surfaces: (a), the surface S_z which is directly in the front of the plate,
 467 of dimensions $0.66 \text{ m} \times 0.6 \text{ m}$ and positioned at $z_v = 0.05 \text{ m}$; (b), the four lateral surfaces
 468 (denoted $S_{x\pm}$, $S_{y\pm}$ as shown in Fig. 9(b)) to enclose the whole panel. The active sound
 469 intensity on S_z was calculated on a grid of 12×10 points uniformly distributed along x
 470 and y , respectively. The sound intensity was only calculated on 10 aligned points on $S_{x\pm}$
 471 uniformly distributed along y and 12 aligned points on $S_{y\pm}$ uniformly distributed along x .
 472 In both case, the points were positioned at $z_v/2$. Note that in the reciprocal approach, the
 473 direction of the active sound intensity is defined by the direction of the force injected by
 474 the dipole (see Fig. 2(f)). To determine the active sound intensity at point \mathbf{x} using the
 475 reciprocity principle, the plate was excited successively by a monopole and dipole source at
 476 point \mathbf{x} .

477 To reduce the number of excitation points and the measurement time, the symmetries
 478 of the system (with respect to $x = L_x/2$ and $y = L_y/2$) were considered. Only the points
 479 belonging to a fourth of Σ_v , as illustrated in Fig. 9(c), were considered, leading to a total of
 480 40 positions of excitation as compared to 160 in Fig. 9(b). The experiment was performed
 481 in an anechoic room, using two translating robots to automate the process (see Figs. 3(b)
 482 and 3(c)). One robot was used to move the monopole source over each point σ_v defining
 483 the discretized surfaces (considering the above symmetry) and the other robot was used to
 484 move a Polytec single-point laser vibrometer measuring the panel velocity on a 15×13 point

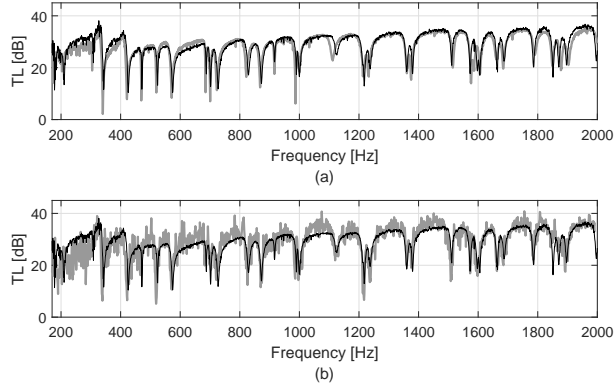


FIG. 10. Transmission loss (dB). (a) numerical approach (bold gray line) vs. experimental reciprocity approach (light black line). (b) transmission loss facility (bold gray line) vs. experimental reciprocity approach (light black line).

485 mesh.

486 As a reference to compare the following numerical and experimental results, a numerical
 487 model has been established to accurately evaluate the radiated power from wall pressure
 488 and wall velocity values. At the wall, the particle velocity sensitivity function H_{v_0} normal
 489 to the plate is equal to the plate velocity sensitivity function H_v . Expressing it in the
 490 wavenumber domain allows using the wavenumber relation between the acoustic pressure
 491 and the particle velocity [23] and thus determining H_p at the wall. Finally, by expressing
 492 Eqs. (4), (5) and (17) in the wavenumber domain and using H_p and H_{v_0} determined at the
 493 wall, one obtains the radiated power directly at the wall.

494 Fig. 10(a) shows experimental results obtained based on the reciprocity method, while
 495 considering the virtual surface Σ_v described at the beginning of this section and illustrated
 496 in Figs. 9(b) and 9(c), versus simulation results for which the radiated power was evaluated
 497 at the panel surface. The curves match very well on the whole frequency range. This
 498 demonstrates that the proposed reciprocity approach accurately reproduces the theoretical
 499 TL for the considered test case. Moreover, it validates the definition of the virtual surface
 500 Σ_v considered in the experiment.

501 The experimental results obtained with the reciprocity principle are compared in Fig. 10(b)
 502 to the experimental results obtained in the transmission loss facility. The transmission loss
 503 facility results are noisier than those derived from the reciprocity principle. A good agree-
 504 ment is however noticed in general. Relatively small differences are noticeable above the

505 Schroeder frequency (410 Hz). These could be explained by the non-perfectly diffuse char-
506 acter of the sound field in the reverberant room. On the other hand, below 410 Hz the TL
507 measured in the transmission loss facility is on average 6.5 dB lower than the one obtained
508 with the reciprocal approach. This is explained by the modal behavior of the reverber-
509 ant room below the Schroeder frequency, which enhances the non diffuse character of the
510 incident sound field.

511 VIII. CONCLUSION

512 In this paper, a methodology for characterizing the response of flat panels to a diffuse
513 acoustic field excitation without using a reverberant room was proposed. This approach is
514 based on the mathematical formulation of the random excitation problem in the wavenum-
515 ber domain. This formulation indicates that the panel's response at point \mathbf{x} (on the panel
516 or in the acoustic medium) to a random field depends on two quantities in the wavenumber
517 domain: the wall-pressure cross spectral density function of the excitation and on so-called
518 'sensitivity functions' at point \mathbf{x} which characterize the panel. Using the reciprocity princi-
519 ple, it has been shown that these functions can be determined from the panel velocity field
520 in the wavenumber domain when the system is excited by a source of unit amplitude at the
521 point of interest \mathbf{x} . The sensitivity functions can be estimated easily by experiment based
522 on the reciprocal interpretation.

523 The proposed approach avoids the use of a reverberant room to determine the sound
524 transmission loss factor and vibration response of plane panels under a diffuse field excitation.
525 As the excitation is represented by an analytical model, this approach can be applied to
526 experimentally characterize the vibroacoustic response of a panel to an ideal diffuse acoustic
527 field. It should however be underlined that the main limitations of the proposed approach
528 rely on the assumptions of the mathematical formulation of the problem: the system should
529 be linear (*i.e.*, elastic material, small deformations) and time invariant, and the condition
530 of a baffled panel in an anechoic environment should be verified (particularly for acoustic
531 applications). It offers however a large field of applications.

532 From a practical point of view, the vibration response of a panel to a diffuse field excitation
533 can be easily estimated using a mechanical source of effort and a vibration measuring device
534 to determine the vibratory response of the panel (in this study, a shaker and a scanning laser

535 vibrometer were used). In this particular case, the use of a baffle is not crucial, because no
536 acoustic excitation are considered.

537 For acoustic applications, the condition of baffled panel in an anechoic environment is
538 fundamental to agree with the assumption of blocked pressure. Monopole and dipole sources
539 are required to determine the radiated pressure and the particle velocity, respectively. It can
540 be quite challenging to experimentally reproduce those sources. In this study, a monopole-
541 like source was used and moved from a certain distance to represent two monopoles close
542 to each other and out of phase. A dipole source could thereby be reproduced. For the
543 determination of the sound transmission loss factor, the monopole and dipole excitations
544 have to be applied on several points discretizing a virtual surface, which encloses the whole
545 panel. For each position of the excitation, the vibration response of the entire panel has to
546 be measured. In this study, two translating robots were used to automate the process. As
547 opposed to measurements in a transmission loss facility, this experiment was highly time-
548 consuming. However, with the recently developed vibration measuring techniques (such as
549 optical measurement), the time of experiment could be largely reduced.

550 To conclude, the method has been validated numerically and experimentally for the
551 considered test case. Comparisons of numerical and experimental results have shown that
552 the sensitivity functions have been well estimated both inside and outside the acoustic circle
553 in the wavenumber domain. A good agreement between numerical and experimental results
554 has also been obtained whether for the velocity spectrum at a point on the panel or for the
555 sound intensity spectrum at a point in the acoustic domain. An application of the proposed
556 methodology for estimating the sound transmission loss of the plate has been presented and
557 the results have been compared with standard measurements in a coupled room facility. In
558 the near future, the method will be extended to the characterization of panels excited by a
559 turbulent boundary layer.

560 **ACKNOWLEDGMENTS**

561 This work was supported by the Labex CeLyA of Université de Lyon, operated by the
562 French National Research Agency (ANR-10-LABX-0060/ANR-11-IDEX-0007).

563 Special thanks must go to Mr Patrick Blachier for his considerable contribution to all

564 experimental setups required to perform this study.

- 565 [1] ISO 10140-2:2010 Acoustics – Laboratory measurement of sound insulation of building ele-
566 ments – Part 2: Measurement of airborne sound insulation (International Standard Organi-
567 zation, Geneva, Switzerland, 2010).
- 568 [2] ASTM E90-09 Standard Test Method for Laboratory Measurement of Airborne Sound Trans-
569 mission Loss of Building Partitions and Elements (ASTM International, West Conshohocken,
570 PA, 2009).
- 571 [3] ISO 15186-1:2000 Acoustics – Measurement of sound insulation in buildings and of building
572 elements using sound intensity – Part 1: Laboratory measurements (International Standard
573 Organization, Geneva, Switzerland, 2000).
- 574 [4] ASTM E2249-02 (2016) Standard Test Method for Laboratory Measurement of Airborne
575 Sound Transmission Loss of Building Partitions and Elements Using Sound Intensity (ASTM
576 International, West Conshohocken, PA, 2016).
- 577 [5] T. Bravo, S. J. Elliott, “Variability of low frequency sound transmission measurements”, *J.*
578 *Acoust. Soc. Am.* **115**(6), 2986-2997 (2004).
- 579 [6] A. Dijckmans, C. Vermeir, “Numerical investigation of the repeatability and reproductibility
580 of laboratory sound insulation measurements”, *Acta Acust. United Ac.* **99**, 421-432 (2013).
- 581 [7] N. Garg, L. Gandhi, A. Kumar, P. Kumar, P. K. Saini, “Measurement uncertainty in air-
582 borne sound insulation and single-number quantities using sound pressure and sound intensity
583 approaches”, *Noise Control Eng. J.* **64**(2), 153-169 (2016).
- 584 [8] W. K. Bonness, D. E. Capone, S. A. Hambric, “Low-wavenumber turbulent boundary layer
585 wall-pressure measurements from vibration data on a cylinder in pipe flow”, *J. Sound Vib.*
586 **329**, 4166–4180 (2010).
- 587 [9] S. A. Hambric, Y. F. Hwang, W. K. Bonness, “Vibrations of plates with clamped and free
588 edges excited by low-speed turbulent boundary layer flow”, *J. Fluid Struct.* **19**, 93–110 (2004).
- 589 [10] O. Robin, A. Berry, S. Moreau, “Experimental vibroacoustic testing of plane panels using
590 synthesized random pressure fields”, *J. Acoust. Soc. Am.* **135**(6), 3434-3445 (2014).
- 591 [11] J-D. Chazot, O. Robin, J-L. Guyader, N. Atalla, “Diffuse Acoustic Field Produced in Re-
592 verberant Rooms: A Boundary Diffuse Field Index”, *Acta Acust. United Ac.* **102**, 503-516

- 593 (2016).
- 594 [12] F. Fahy, "Sound Intensity", pp. 96, Elsevier Applied Science, London (1989).
- 595 [13] C. Maury, P. Gardonio, S. J. Elliott, "A wavenumber approach to modelling the response of
596 a randomly excited panel, part 1: general theory", J. Sound Vib. **252**(1), 83-113 (2002).
- 597 [14] Y. K. Lin, "Probabilistic theory of structural dynamics", pp. 207, McGraw-Hill, New York
598 (1967).
- 599 [15] R. K. Cook, R. V. Waterhouse, R. D. Berendt, S. Edelman, M. C. Thompson Jr, "Measurement
600 of correlation coefficients in reverberant sound fields", J. Acoust. Soc. Am. **27**(6), 1072-1077
601 (1955).
- 602 [16] F. J. Fahy, "Some Applications of the Reciprocity Principle in Experimental Vibroacoustics",
603 Acoustical Physics **49**(2), 217-229 (2003).
- 604 [17] L. Maxit, V. Denis, "Prediction of flow induced sound and vibration of periodically stiffened
605 plates", J. Acoust. Soc. Am. **133**(1), 146-160 (2013).
- 606 [18] L. M. Lyamshev, "A method for solving the proble; of sound radiation by thin elastic shells
607 and plates", Sov. Phys. Acoust. **102**(5), 122-124 (1958).
- 608 [19] O. Robin, J-D. Chazot, R. Boulandet, M. Michau, A. Berry, N. Atalla, "A plane and thin
609 panel with representative simply supported boundary conditions for laboratory vibroacoustic
610 test", Acta Acust. United Ac. **102**(1), 170-182 (2016).
- 611 [20] H. -J. Kang, J. -G. Ih, H. -S. Kim, J. -S. Kim "An experimental investigation on the directional
612 distribution of incident energy for the prediction of sound transmission loss", Applied Acoustics
613 **63**, 283-294 (2002).
- 614 [21] N. H. Schiller, A. R. Allen, "Assessment of analytical predictions for diffuse field sound trans-
615 mission loss", *In proceedings of the 44th InterNoise Congress*, Paper No. IN15.257, pp. 5971-
616 5982, San Francisco, California, USA (2015).
- 617 [22] R. W. Guy, A. De Mey, "Measurement of sound transmission loss by sound intensity", Cana-
618 dian Acoustics **13**(2), 25-44 (1985).
- 619 [23] E. G. Williams, J. D. Maynard, "Numerical evaluation of the Rayleigh integral for planar
620 radiators using the FFT", J. Acoust. Soc. Am. **72**(6), 2020-2030 (1982).
- 621 [24] A. D. Pierce, "Acoustics: An Introduction to Its Physical Principles and Applications", pp.
622 165-167, Acoustical Society of America, New York (1989).

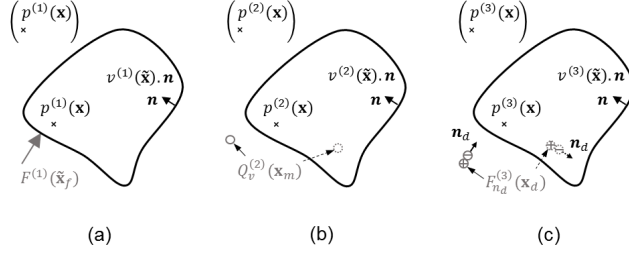


FIG. 11. Illustration of the three considered vibroacoustic problems of an elastic structure excited by: (a) a normal force at point $\tilde{\mathbf{x}}_f$, (b) a monopole source at point \mathbf{x}_m (internal or external to the structure), (c) a dipole source at point \mathbf{x}_d (internal or external to the structure).

623 **Appendix A: Acoustic reciprocity principles: mathematical formulation of the dif-**
624 **ferent vibroacoustic problems**

625 Let's consider a thin elastic structure in an acoustic medium of fluid density ρ_0 where
626 sound waves propagate at a certain speed c_0 . The vibroacoustic response of a structure at
627 any given point $\mathbf{x} = (x, y, z)$ (belonging to the acoustic medium or the structure) is studied
628 for three separate loadings (as illustrated in Fig. 11):

- 629 1. a normal point force at point $\tilde{\mathbf{x}}_f$,
- 630 2. a monopole source at point \mathbf{x}_m ,
- 631 3. a dipole source at point \mathbf{x}_d ,

632 where points belonging to the structure are denoted $\tilde{\mathbf{x}}$.

633 Any kind of thin elastic structure can be considered; and the excitation and observation
634 point $(p^{(i)}(\mathbf{x}), i = 1, 2 \text{ or } 3)$ can either be internal or external to the structure. It is also
635 assumed that there is no other acoustic loading on the other side of the structure. The
636 monopole source can be introduced in the Helmholtz equation by a Dirac function at point
637 \mathbf{x}_m . As a dipole source is defined by two monopoles separated by a distance d (supposedly
638 small compared to the acoustic wavelength) and out of phase, a dipole source is introduced
639 by the gradient of a Dirac at point \mathbf{x}_d in direction \mathbf{n}_d . Sticking to the above numbering for
640 each load case, the Helmholtz equations are given by

$$\Delta p^{(1)}(\mathbf{x}) + k_0^2 p^{(1)}(\mathbf{x}) = 0, \quad (\text{A1})$$

$$\Delta p^{(2)}(\mathbf{x}) + k_0^2 p^{(2)}(\mathbf{x}) = -j\omega\rho_0 Q_v^{(2)} \delta(\mathbf{x} - \mathbf{x}_m), \quad (\text{A2})$$

$$\Delta p^{(3)}(\mathbf{x}) + k_0^2 p^{(3)}(\mathbf{x}) = -F_{n_d}^{(3)} \frac{\partial}{\partial \mathbf{n}_d} \delta(\mathbf{x} - \mathbf{x}_d) [24], \quad (\text{A3})$$

641 where ω is the angular frequency, Q_v the volume velocity flow of the monopole source,
 642 $F_{n_d}^{(3)} = j\omega\rho_0 dQ_v^{(3)}$ the dipole source strength (or dipole force) and $k_0 = \omega/c_0$ the acoustic
 643 wavenumber. The equilibrium equation for the structure in each case is

$$Lv^{(1)}(\tilde{\mathbf{x}}) = F^{(1)} \delta(\tilde{\mathbf{x}} - \tilde{\mathbf{x}}_f) - p^{(1)}(\tilde{\mathbf{x}}), \quad (\text{A4})$$

$$Lv^{(2)}(\tilde{\mathbf{x}}) = -p^{(2)}(\tilde{\mathbf{x}}), \quad (\text{A5})$$

$$Lv^{(3)}(\tilde{\mathbf{x}}) = -p^{(3)}(\tilde{\mathbf{x}}), \quad (\text{A6})$$

644 where L is the self-adjoint operator of the structure and v is the structure velocity in direction
 645 \mathbf{n} normal to the structure. Euler's formula provides a relation between the pressure gradient
 646 in the fluid and the velocity along the normal external to the fluid. On the surface of the
 647 structure, the normal external to the fluid corresponds to $-\mathbf{n}$. In this particular case, Euler's
 648 formula becomes

$$\frac{\partial p}{\partial \mathbf{n}}(\tilde{\mathbf{x}}) = j\omega\rho_0 v(\tilde{\mathbf{x}}). \quad (\text{A7})$$

649 1. Reciprocity principle for the radiated pressure (monopole source)

650 Multiplying Eq. (A1) by $p^{(2)}(\mathbf{x})$ and Eq. (A2) by $-p^{(1)}(\mathbf{x})$, adding them and integrating
 651 them over the entire acoustic domain, one obtains

$$\int_V [\Delta p^{(1)}(\mathbf{x}) p^{(2)}(\mathbf{x}) - \Delta p^{(2)}(\mathbf{x}) p^{(1)}(\mathbf{x})] d\mathbf{x} = j\omega\rho_0 Q_v^{(2)} \int_V p^{(1)}(\mathbf{x}) \delta(\mathbf{x} - \mathbf{x}_m) d\mathbf{x}. \quad (\text{A8})$$

652 The volume integral on the left-hand side of Eq. (A8) can be transformed to a surface in-
 653 tegral using Green's theorem. Then, using Euler's formula together with Eqs. (A4) and (A5),

654 one finally obtains [18]

$$F^{(1)} \int_S \frac{\partial p^{(2)}}{\partial \mathbf{n}}(\tilde{\mathbf{x}}) \delta(\tilde{\mathbf{x}} - \tilde{\mathbf{x}}_f) d\tilde{\mathbf{x}} = j\omega\rho_0 Q_v^{(2)} \int_V p^{(1)}(\mathbf{x}) \delta(\mathbf{x} - \mathbf{x}_m) d\mathbf{x}. \quad (\text{A9})$$

655 From the property of the Dirac delta function (*i.e.*, $\int_V f(\mathbf{x}) \delta(\mathbf{x} - \mathbf{x}_0) d\mathbf{x} = f(\mathbf{x}_0)$ for
656 any function f defined on V and any point $\mathbf{x}_0 \in V$) one has:

$$F^{(1)} \frac{\partial p^{(2)}}{\partial \mathbf{n}}(\tilde{\mathbf{x}}_f) = j\omega\rho_0 Q_v^{(2)} p^{(1)}(\mathbf{x}_m). \quad (\text{A10})$$

657 Using Eq. (A7), Eq. (A10) becomes

$$\frac{p^{(1)}}{F^{(1)}}(\mathbf{x}_m) = \frac{v^{(2)}}{Q_v^{(2)}}(\tilde{\mathbf{x}}_f). \quad (\text{A11})$$

658 Eq. (A11) shows that the pressure radiated by a structure at point \mathbf{x}_m when it is excited
659 by a normal unit point force at point $\tilde{\mathbf{x}}_f$ equals the structure normal velocity at point $\tilde{\mathbf{x}}_f$
660 when it is excited by a monopole source of unit volume velocity at point \mathbf{x}_m .

661 2. Reciprocity principle for the particle velocity (dipole source)

662 Multiplying Eq. (A1) by $p^{(3)}(\mathbf{x})$ and Eq. (A3) by $-p^{(1)}(\mathbf{x})$, adding them and integrating
663 them over the entire acoustic domain, one obtains

$$\int_V [\Delta p^{(1)}(\mathbf{x}) p^{(3)}(\mathbf{x}) - \Delta p^{(3)}(\mathbf{x}) p^{(1)}(\mathbf{x})] d\mathbf{x} = F_{n_d}^{(3)} \int_V p^{(1)}(\mathbf{x}) \frac{\partial}{\partial \mathbf{n}_d} \delta(\mathbf{x} - \mathbf{x}_d) d\mathbf{x}. \quad (\text{A12})$$

664 As previously, the volume integral on the left-hand side of Eq. (A12) can be transformed
665 to a surface integral using Green's theorem. Then, using Euler's formula together with
666 Eqs. (A4) and (A6), one finally obtains [18]

$$F^{(1)} \int_S \frac{\partial p^{(3)}}{\partial \mathbf{n}}(\tilde{\mathbf{x}}) \delta(\tilde{\mathbf{x}} - \tilde{\mathbf{x}}_f) d\tilde{\mathbf{x}} = F_{n_d}^{(3)} \int_V p^{(1)}(\mathbf{x}) \frac{\partial}{\partial \mathbf{n}_d} \delta(\mathbf{x} - \mathbf{x}_d) d\mathbf{x}, \quad (\text{A13})$$

667 Using the previously described property of the Dirac delta function and the property
668 of the distributional derivative of the Dirac delta function (*i.e.*, $\int_V f(\mathbf{x}) \frac{\partial}{\partial \mathbf{n}} \delta(\mathbf{x} - \mathbf{x}_0) d\mathbf{x} =$
669 $-\int_V \frac{\partial}{\partial \mathbf{n}} f(\mathbf{x}) \delta(\mathbf{x} - \mathbf{x}_0) d\mathbf{x} = -\frac{\partial}{\partial \mathbf{n}} f(\mathbf{x}_0)$ for any function f defined on V and any point

670 $\mathbf{x}_0 \in V$) Eq. (A13) becomes

$$F^{(1)} \frac{\partial p^{(3)}}{\partial \mathbf{n}} (\tilde{\mathbf{x}}_f) = -F_{n_d}^{(3)} \frac{\partial p^{(1)}}{\partial \mathbf{n}_d} (\mathbf{x}_d). \quad (\text{A14})$$

671 Using Euler's formula, the normal velocity of the structure at point $\tilde{\mathbf{x}}_f$ and the particle
672 velocity v_{n_d} in direction \mathbf{n}_d at point \mathbf{x}_d are introduced in Eq. (A14). One finally obtains

$$\frac{v_{n_d}^{(1)}}{F^{(1)}} (\mathbf{x}_d) = \frac{v^{(3)}}{F_{n_d}^{(3)}} (\tilde{\mathbf{x}}_f). \quad (\text{A15})$$

673 Eq. (A15) shows that the particle velocity in direction \mathbf{n}_d at point \mathbf{x}_d in the acoustic
674 medium when the structure is excited by a normal unit point force at point $\tilde{\mathbf{x}}_f$ equals the
675 structure normal velocity at point $\tilde{\mathbf{x}}_f$ when it is excited by a dipole source at point \mathbf{x}_d
676 oriented in direction \mathbf{n}_d and of unit injected force.

677 **Appendix B: Numerical simulations**

678 The panel vibratory response should be estimated numerically for the four different
679 cases of excitation: (a) a wall plane wave for $H_\alpha(\mathbf{x}, \mathbf{k}, \omega)$; (b) a normal point force
680 for $H_{v/F_n}(\tilde{\mathbf{x}}, \mathbf{x}, \omega)$; (c) a monopole source for $H_{v/Q_v}(\tilde{\mathbf{x}}, \mathbf{x}, \omega)$; (d) a dipole source for
681 $H_{v/F_0}(\tilde{\mathbf{x}}, \mathbf{x}, \omega)$. They can be estimated by neglecting the fluid-structure interaction and
682 considering the modal expansion technique. For a panel that has simply supported bound-
683 ary conditions on all of its edges, the modal angular frequency ω_{mn} , the spatial mode shape
684 ϕ_{mn} , and the modal mass M_{mn} for the (m, n) mode are given, respectively, by

$$\omega_{mn} = \left[\left(\frac{m\pi}{L_x} \right)^2 + \left(\frac{n\pi}{L_y} \right)^2 \right] \sqrt{\frac{D}{\rho h}}, \quad (\text{B1})$$

$$\phi_{mn}(\mathbf{x}) = \sin\left(\frac{m\pi}{L_x}x\right) \sin\left(\frac{n\pi}{L_y}y\right), \quad (\text{B2})$$

$$M_{mn} = \frac{\rho h L_x L_y}{4}, \quad (\text{B3})$$

687 where m and n are non-zero strictly positive integers. The normal velocity v of the plate

688 excited by the pressure distribution $P(\tilde{\mathbf{x}})$, $\tilde{\mathbf{x}} \in \Sigma_p$ is then obtained with:

$$v(\mathbf{x}, \omega) = j\omega \sum_{m,n} \frac{\mathbf{F}_{mn} \phi_{mn}(\mathbf{x})}{M_{mn} (\omega_{mn}^2 - \omega^2 + j\eta\omega\omega_{mn})}, \quad (\text{B4})$$

689 where the modal force \mathbf{F}_{mn} is defined by

$$\mathbf{F}_{mn} = \int_{\Sigma_p} P(\tilde{\mathbf{x}}) \phi_{mn}(\tilde{\mathbf{x}}) d\tilde{\mathbf{x}}. \quad (\text{B5})$$

690 1. Calculation of the sensitivity functions with the direct interpretation

691 The direct interpretation described in Sec. III and in Fig. 2 indicates that the sensi-
 692 tivity functions are equal to the system response at point \mathbf{x} when the panel is excited by
 693 wall-pressure plane waves of wavenumber $-\mathbf{k} = (-k_x, -k_y)$. The modal force is therefore
 694 calculated by considering the pressure distribution $P(\tilde{\mathbf{x}}) = e^{-j\mathbf{k}\tilde{\mathbf{x}}}$. In this case, the analytical
 695 solution to Eq. (B5) is

$$\mathbf{F}_{mn} = I_m^x I_n^y, \quad (\text{B6})$$

696 where for $\xi = x$ or $\xi = y$,

$$I_p^\xi = \begin{cases} \left(\frac{p\pi}{L_\xi}\right) \frac{(-1)^p e^{-jk_\xi L_\xi} - 1}{k_\xi^2 - \left(\frac{p\pi}{L_\xi}\right)^2}, & \text{if } |k_\xi| \neq \frac{p\pi}{L_\xi} \\ \frac{1}{2} j L_\xi, & \text{otherwise.} \end{cases} \quad (\text{B7})$$

697 The sensitivity functions H_v for a point \mathbf{x} on the panel can be directly estimated using
 698 Eqs. (B4) to (B7). Based on the velocity response of the plate to a wall-pressure plane
 699 wave, the radiated pressure at a point \mathbf{x} in the acoustic domain may be calculated using the
 700 Rayleigh integral [23] whereas the particle velocity may be deduced from the Euler equation.
 701 Doing so for a set of wall-pressure plane waves allows calculating the sensitivity functions
 702 H_p and H_{v0} at point \mathbf{x} in the acoustic domain.

703 2. Calculation of the sensitivity functions with the reciprocity interpretation

704 The calculation of the velocity sensitivity function H_v at point \mathbf{x} using the reciprocity
 705 principle involves exciting the plate with a normal unit force at point \mathbf{x} . The modal force is

706 thus simply given by

$$\mathbf{F}_{mn} = \phi_{mn}(\mathbf{x}). \quad (\text{B8})$$

707 According to the process described in Sec. V, the normal velocity of the panel should be
 708 calculated with Eq. (B4) for points $\tilde{\mathbf{x}} \in \Gamma_{\tilde{\mathbf{x}}}$. A discrete Fourier transform is then applied to
 709 deduce the sensitivity functions $H_v(\mathbf{x}, \mathbf{k}, \omega)$.

710 Similarly, the pressure sensitivity function H_p at point \mathbf{x} in the acoustic domain is ob-
 711 tained by exciting the plate by a monopole at point \mathbf{x} . The particle velocity sensitivity
 712 function H_{v_0} at point \mathbf{x} is obtained analogously using a dipole excitation in the direction
 713 \mathbf{n} at point \mathbf{x} . The modal force is then obtained by approximating the integral of Eq. (B5)
 714 with the rectangular integration rule for a wall-pressure defined by

$$P(\tilde{\mathbf{x}}) = j\omega\rho_0 Q_v \frac{e^{-jk_0 r}}{2\pi r} \quad (\text{B9})$$

715 for the monopole case, with $r = |\mathbf{x} - \tilde{\mathbf{x}}|$ and $Q_v = 1 \text{ m}^3 \cdot \text{s}^{-1}$. For the dipole case,

$$P(\tilde{\mathbf{x}}) = \frac{F_0}{d} \left(\frac{e^{-jk_0 r_1}}{2\pi r_1} - \frac{e^{-jk_0 r_2}}{2\pi r_2} \right). \quad (\text{B10})$$

716 where r_1 and r_2 are two positions of monopoles separated by a distance d representing a
 717 dipole at a distance r [24] and the dipole force will be then considered of unit amplitude
 718 (*i.e.*, $F_0 = 1 \text{ N}$).

719 Fig. 1. Panel (gray line) and coordinate system. (a) receiving side: semi-infinite
 720 domain. (b) source side: theoretical DAF.

721 Fig. 2. Direct interpretation of the sensitivity functions: (a) H_v , (c) H_p , (e) H_{v_0}
 722 and corresponding reciprocal interpretation (b) H_v , (d) H_p , (f) H_{v_0} . (d) and (f) see
 723 appendix for demonstration.

724 Fig. 3. Experimental setup. (a) plate excited by a shaker to determine H_v . (b) and
 725 (c) baffled plate excited by a monopole source to determine H_p and H_{v_0} . 1 - shaker
 726 with impedance head. 2 - plate. 3 - frame. 4 - baffle. 5 - sound absorbing foam. 6 -
 727 monopole source mounted on 3-axis robot. 7 - single-point laser vibrometer mounted
 728 on 2-axis robot.

729 Fig. 4. Velocity sensitivity functions at point \mathbf{x}_M , $|H_v|^2$ (dB, ref. $1 \text{ m}^2 \cdot \text{s}^{-2}$): direct
 730 calculation (left), numerical reciprocity approach (middle), experimental reciprocity
 731 approach (right). (a) $f = 178 \text{ Hz}$. (b) $f = 600 \text{ Hz}$. (c) $f = 1710 \text{ Hz}$. - - -, circle of
 732 radius k_f . —, circle of radius k_0 .

733 Fig. 5. Product of sensitivity functions at point \mathbf{x}_N , $|\text{Re}\{H_p \times H_{v_0}^*\}|$ (dB, ref.
 734 $1 \text{ Pa} \cdot \text{m} \cdot \text{s}^{-1}$): direct calculation (left), numerical reciprocity approach (middle), ex-
 735 perimental reciprocity approach (right). (a) $f = 178 \text{ Hz}$. (b) $f = 600 \text{ Hz}$. (c)
 736 $f = 1710 \text{ Hz}$. - - -, circle of radius k_f . —, circle of radius k_0 .

737 Fig. 6. Velocity ASD functions G_{vv} (dB, ref. $1 \text{ m}^2 \cdot \text{s}^{-2} \cdot \text{Hz}^{-1}$). (a) direct calculation
 738 (bold gray line) vs. numerical reciprocity approach (light black line). (b) numerical
 739 reciprocity approach (bold gray line) vs. experimental reciprocity approach (light
 740 black line).

741 Fig. 7. Pressure – particle velocity CSD functions $\text{Re}\{G_{pv_0}\}$ (dB, ref. $1 \text{ W}^2 \cdot \text{m}^{-2} \cdot \text{Hz}^{-1}$).
 742 (a) direct calculation (bold gray line) vs. numerical reciprocity approach (light black
 743 line). (b) numerical reciprocity approach (bold gray line) vs. experimental reciprocity
 744 approach (light black line).

745 Fig. 8. Velocity ASD functions G_{vv} (dB, ref. $1 \text{ m}^2 \cdot \text{s}^{-2} \cdot \text{Hz}^{-1}$): reverberant room
 746 measurements (bold gray line) vs. experimental reciprocity approach (light black
 747 line).

748 Fig. 9. Illustration of the virtual surface Σ_v considered for estimating the radiated
749 power. (a) in the transmission loss facility. (b) with the reciprocal approach. (c) with
750 the reciprocal approach considering the symmetry properties of the system.

751 Fig. 10. Transmission loss (dB). (a) numerical approach (bold gray line) vs. experi-
752 mental reciprocity approach (light black line). (b) transmission loss facility (bold gray
753 line) vs. experimental reciprocity approach (light black line).

754 Fig. 11. Illustration of the three considered vibroacoustic problems of an elastic struc-
755 ture excited by: (a) a normal force at point $\tilde{\mathbf{x}}_f$, (b) a monopole source at point \mathbf{x}_m
756 (internal or external to the structure), (c) a dipole source at point \mathbf{x}_d (internal or
757 external to the structure).

TABLE I. Properties of the simply supported aluminum plate.

Parameter (Symbol), Unit	Value
Young's modulus (E), GPa	68.9
Poisson's ratio (ν)	0.3
Mass density (ρ), kg/m ³	2740
Length (L_x), mm	480
Width (L_y), mm	420
Thickness (h), mm	3.17